distribution of redox system-related enzymes in the livers was immunohistochemically absent, and the hepatocytes expressing the redox-related enzymes and those not expressing these enzymes were intermingled in various ratios. The hepatocytes that overexpressed the redox system-related enzymes were evident among the hepatocytes expressing these enzymes. In addition to these immunohistochemical data, Western blot results also supported the observation that the redox system-related enzymes were overinduced in some hepatocytes. Overinduction of redox system-related enzymes in the hepatocytes was observed around the time of clinical onset. By marked contrast, the SOD1-mutated motor neurons that formed inclusions showed intra-inclusional co-aggregation of redox proteins with SOD1, thereby reducing the availability of the redox system (Kato et al., 2004). Among motor neurons without inclusions, some exposed to mutant SOD1 stress (i.e., ALS stress) are capable of overexpressing redox system-related enzymes as one of their vital physiological reactions, although many SOD1-mutated motor neurons showed disruption of the redox system (Kato et al., 2005). Neurons under long-term ALS stress no longer have the ability to upregulate the redox system, and as ALS progresses, these residual ALS neurons finally become unable even to maintain the redox system itself (Kato et al., 2005). Therefore, unlike the situation in hepatocytes, breakdown of the redox system in SOD1-mutated motor neurons results in cell death. The redox system-related enzymes that are abundant in the liver (Immenschuh et al., 2003) convert superoxide radicals into hydrogen peroxide that is immediately converted by SOD1 to harmless water and oxygen. Because SOD1 is rich in the liver under physiological conditions (Marklund, 1980), mutant SOD1 is also induced abundantly in the liver of ALS model animals with the SOD1 gene mutation. Although hepatocytes in G1H-G93A mice are exposed to mutant SOD1 stress throughout life, in order to protect themselves from the mutant SOD1 stress, these hepatocytes are able to keep on inducing the redox system-related enzymes and maintaining the redox system. However, it is considered impossible for hepatocytes under long-term mutant SOD1 stress to keep on inducing these redox system-related enzymes. Therefore, hepatocytes under long-term mutant SOD1 stress, e.g., the hepatocytes in the FALS patient with the 11-year disease course and in the end-stage G1L-G93A mice, eventually become unable to maintain the redox system. On the other hand, there are many reports that diverse stresses dangerous to cell survival result in the overinduction of redox system-related enzymes, contributing to the regulation of signal transduction (Andoh et al., 2003; Biteau et al., 2003; Georgiou, 2003; Neuman et al., 2003; Wood et al., 2003; Chang et al., 2004). This redox signal transduction is linked to important systems such as cellular differentiation, immune response, growth control, apoptosis, and tumor growth (Jin et al., 1997; Berggren et al., 2001; Koo et al., 2002; Chang et al., 2002; Mu et al., 2002; Neuman et al., 2003). Redox system-related enzymes are overinduced in reaponse to survival-threatening stresses such as mutant SOD1. Our findings suggest that the up-regulation of redox system-related enzymes may rescue cells from death under mutant SOD1 stress. Therefore, we postulate that our data will lead to the development of a new therapy based on redox system up-regulation for the treatment of ALS, which for over 130 years has had an unknown etiology.

Acknowledgments. This study was supported in part by a Grant-in-Aid for Scientific Research (c) (S.K.: 17500229) and a Grant-in-Aid for Scientific Research in Priority Area (T.N.) from the Ministry of Education, Culture, Sports, Science and Technology of Japan, by a Research Grant on Measures for Intractable Diseases from the Ministry of Health, Labour and Welfare of Japan (S.K. and Y.I.), and by a Grant from Research on Psychiatric and Neurological Disease and Mental Health (S.K., M.A. and Y.I.)

References

Abe Y. and Okazaki T. (1987). Purification and properties of the manganese superoxide dismutase from the liver of bullfrog, Rana catesbeiana. Arch. Biochem. Biophys. 253, 241-248.

Andoh T., Chiueh C.C. and Chock P.B. (2003). Cyclic GMP-dependent protein kinase regulates the expression of thioredoxin and thioredoxin peroxidase-1 during hormesis in response to oxidative stress-induced apoptosis. J. Biol. Chem. 278, 885-890.

Berggren M.I., Husbeck B., Samulitis B., Baker A.F., Gallegos A. and Powis G. (2001). Thioredoxin peroxidase-1 (peroxiredoxin-1) is increased in thioredoxin-1 transfected cells and results in enhanced protection against apoptosis caused by hydrogen peroxide but not by other agents including dexamethasone, etoposide, and doxorubicin. Arch. Biochem. Biophys. 392,103-109.

Biteau B., Labarre J. and Toledano M.B. (2003). ATP-dependent reduction of cysteine-sulphinic acid by S. cerevisiae sulphiredoxin. Nature 425, 980-984.

Chae H.Z., Kim I.H., Kim K. and Rhee S.G. (1993). Cloning, sequencing, and mutation of thiol-specific antioxidant gene of Saccharomyces cerevisiae. J. Biol. Chem. 268, 16815-16821.

Chae H.Z., Robison K., Poole L.B., Church G., Storz G. and Rhee S.G. (1994). Cloning and sequencing of thiol-specific antioxidant from mammalian brain: alkyl hydroperoxide reductase and thiol-specific antioxidant define a large family of antioxidant enzymes. Proc. Natl. Acad. Sci. USA 91, 7017-7021.

Chang T.S., Jeong W., Choi S.Y., Yu S., Kang S.W. and Rhee S.G. (2002). Regulation of peroxiredoxin I activity by cdc2-mediated phosphorylation. J. Biol. Chem. 277, 25370-25376.

Chang T.S., Jeong W., Woo H.A., Lee S.M., Park S. and Rhee S.G. (2004). Characterization of mammalian sulfiredoxin and its reactivation of hyperoxidized peroxiredoxin through reduction of cysteine sulfinic acid in the active site to cysteine. J. Biol. Chem. 279, 50994-51001.

Charcot J.M. and Joffroy A. (1869). Deux cas d'atrophie musculaire progressive avec lésions de la substance grise et des faisceaux antéro-latéraux de la moelle épinière. Arch. Physiol. (Paris) 2, 744-760.

Dal Canto M.C. and Gurney M.E. (1995). Neuropathological changes in

two lines of mice carrying a transgene for mutant human Cu,Zn SOD, and in mice overexpressing wild type human SOD: a model of familial amyotrophic lateral sclerosis (FALS). Brain Res. 676, 25-40.

de Belleroche J., Orrell R.W. and Virgo L. (1996). Amyotrophic lateral sclerosis: recent advances in understanding disease mechanisms. J. Neuropathol. Exp. Neurol. 55, 747-757.

de Haan J.B., Bladier C., Griffiths P., Kelner M., O'Shea R.D., Cheung N.S., Bronson R.T., Silvestro M.J., Wild S., Zheng S.S., Beart P.M., Hertzog P.J. and Kola I. (1998). Mice with a homozygous null mutation for the most abundant glutathione peroxidase, Gpx1, show increased susceptibility to the oxidative stress-inducing agents paraquat and hydrogen peroxide. J. Biol. Chem. 273, 22528-22536.

Deng H.X., Hentati A., Tainer J.A., Iqbal Z., Cayabyab A., Hung W.Y., Getzoff E.D., Hu P., Herzfeldt B., Roos R.P., Warner C., Deng G., Soriano E., Smyth C., Parge H.E. Ahmed A., Roses A.D., Hallewell R.A., Pericak-Vance M.A and Siddique T. (1993). Amyotrophic lateral sclerosis and structural defects in Cu,Zn superoxide dismutase. Science 261, 1047-1051.

Fridovich I. (1986). Superoxide dismutases. Adv. Enzymol. Relat. Area Mol. Biol. 58, 61-97.

Georgiou G. and Masip L. (2003). An overoxidation journey with a return ticket. Science 300, 592-594.

Gurney M.E., Pu H., Chiu A.Y., Dal Canto M.C., Plochow C.W., Alexander D.D., Caliendo J., Hentati A., Kwon Y.W., Deng H.X., Chen W., Zhai P., Sufit R.L. and Siddique T. (1994). Motor neuron degeneration in mice that express a human Cu,Zn superoxide dismutase mutation. Science 264, 1772-1775.

Hirano A. (1996). Neuropathology of ALS: an overview. Neurology 47, S63-66.

Hirotsu S., Abe Y., Nagahara N., Hori H., Nishino T., Okada K. and Hakoshima T. (1999a). Crystallographic characterization of a stress-induced multifunctional protein, rat HBP-23. J. Struct. Biol. 126, 80-83.

Hirotsu S., Abe Y., Okada K., Nagahara N., Hori H., Nishino T. and Hakoshima T. (1999b). Crystal structure of a multifunctional 2-Cys peroxiredoxin heme-binding protein 23 kDa/proliferation-associated gene product. Proc. Natl. Acad. Sci. USA 96,12333-12338.

Hofmann B., Hecht H.J. and Flohe H. (2002). Peroxiredoxins. Biol. Chem. 383, 347-364.

Hudson A.J. (1981). Amyotrophic lateral sclerosis and its association with dementia, parkinsonism and other neurological disorders: a review. Brain 104, 217-247.

Immenschuh S., Baumgart-Vogt E., Tan M., Iwahara S., Ramadori G. and Fahimi H.D. (2003). Differential cellular and subcellular localization of heme-binding protein 23/peroxiredoxin I and heme oxygenase-1 rat liver. J. Histochem. Cytochem. 51, 1621-1631.

Iwahara S., Satoh H., Song D.X., Webb J., Burlingame A.L., Nagae Y. and Muller-Eberhard U. (1995). Purification, characterization, and cloning of a heme-binding protein (23 kDa) in rat liver cytosol. Biochemistry 34, 13398-13406.

Jin D.Y., Chae H.Z., Rhee S.G. and Jeang K.T. (1997). Regulatory role for a novel human thioredoxin peroxidase in NF-kappaB activation. J. Biol. Chem. 272, 30952-30961.

Juneja T., Pericak-Vance M.A., Laing N.G., Dave S. and Siddique T. (1997). Prognosis in familial amyotrophic lateral sclerosis: progression and survival in patients with glu100gly and ala4val mutations in Cu,Zn superoxide dismutase. Neurology 48, 55-57.

Kato S., Shimoda M., Watanabe Y., Nakashima K., Takahashi K. and Ohama E. (1996). Familial amyotrophic lateral sclerosis with a two base pair deletion in superoxide dismutase 1 gene: multisystem degeneration with intracytoplasmic hyaline inclusions in astrocytes. J. Neuropathol. Exp. Neurol. 55,1089-1101.

Kato S., Hayashi H., Nakashima K., Nanba E., Kato M., Hirano A., Nakano I., Asayama K. and Ohama E. (1997). Pathological characterization of astrocytic hyaline inclusions in familial amyotrophic lateral sclerosis. Am. J. Pathol. 151, 611-620.

Kato S., Saito M., Hirano A. and Ohama E. (1999). Recent advances in research on neuropathological aspects of familial amyotrophic lateral sclerosis with superoxide dismutase 1 gene mutations: neuronal Lewy body-like hyaline inclusions and astrocytic hyaline inclusions. Histol. Histopathol. 14, 973-989.

Kato S., Takikawa M., Nakashima K., Hirano A., Cleveland D.W., Kusaka H., Shibata N., Kato M., Nakano I. and Ohama E. (2000). New consensus research on neuropathological aspects of familial amyotrophic lateral sclerosis with superoxide dismutase 1 (SOD1) gene mutations: Inclusions containing SOD1 in neurons and astrocytes. ALS Other Motor Neuron Disorders 1, 163-184.

Kato S., Shaw P., Wood-Allum C., Leigh P.N. and Show C. (2003). Amyotrophic lateral sclerosis, In: Nerodegeneration: The molecular pathology of dementia and movement disorders. Dickson D. (ed) ISN Neuropath Press, Basel. pp 350-368.

Kato S., Saeki Y., Aoki M., Nagai M., Ishigaki A., Itoyama Y., Kato M., Asayama K., Awaya A., Hirano A. and Ohama E. (2004). Histological evidence of redox system breakdown caused by superoxide dismutase 1 (SOD1) aggregation is common to SOD1-mutated motor neurons in humans and animal models. Acta Neuropathol. 107, 149-158.

Kato S., Kato M., Abe Y., Matsumura T., Nishino T., Aoki M., Itoyama Y., Asayama K., Awaya A., Hirano A and Ohama E. (2005). Redox system expression in the motor neurons in amyotrophic lateral sclerosis (ALS): immunohistochemical studies on sporadic ALS, superoxide dismutase 1 (SOD1)-mutated familial ALS, and SOD1-mutated ALS animal models. Acta Neuropathol. 110, 101-112.

Koo K.H., Lee S., Jeong S.Y., Kim E.T., Kim H.J., Kim K., Song K. and Chae H.Z. (2002). Regulation of thioredoxin peroxidase activity by c-terminal truncation. Arch. Biochem. Biophys. 397, 312-318.

Marklund S. (1980). Distribution of CuZn superoxide dismutase and Mn superoxide dismutase in human tissues and extracellular fluids. Acta Physiol. Scand. Suppl. 492,19-23.

Matsumoto A., Okado A., Fujii T., Fujii J., Egashira M., Niikawa N. and Taniguchi N. (1999). Cloning of the peroxiredoxin gene family in rats and characterization of the fourth member. FEBS Lett. 443, 246-250.

Mu Z.M., Yin X.Y. and Prochownik E.V. (2002). Pag, a putative tumor suppressor, interacts with the myc box II domain of c-myc and selectively alters its biological function and target gene expression. J. Biol. Chem. 277, 43175-43184.

Nagai M., Aoki M., Miyoshi I., Kato M., Pasinelli P., Kasai N., Brown Jr R.H. and Itoyama Y. (2001). Rats expressing human cytosolic copper-zinc superoxide dismutase transgenes with amyotrophic lateral sclerosis: associated mutations develop motor neuron disease. J. Neurosci. 21, 9246-9254.

Nakano Y., Hirayama K. and Terao K. (1987). Hepatic ultrastructural changes and liver dysfunction in amyotrophic lateral sclerosis. Arch. Neurol. 44, 103-106.

Neumann C.A., Krause D.S., Carman C.V., Das S., Dubey D.P., Abraham J.L., Bronson R.T., Fujiwara Y., Orkin S.H. and Van Etten R.A. (2003). Essential role for the peroxiredoxin prdx1 in erythrocyte

antioxidant defence and tumour suppression. Nature 424, 561-565.

Prosperi M.T, Ferbus D., Karczinski I. and Goubin G. (1993). A human cDNA corresponding to a gene overexpressed during cell proliferation encodes a product sharing homology with amoebic and bacterial proteins. J. Biol. Chem. 268, 11050-11056.

Rosen D.R., Siddique T., Patterson D., Figlewicz D.A., Sapp P., Hentati A., Donaldson D., Goto J., O'Regan J.P., Deng H.-X., Rahmani Z., Krizus A., McKenna-Yasek D., Cayabyab A., Gaston S.M., Berger R., Tanzi R.E., Halperin J.J., Herzfeldt B., Van den Bergh R., Hung W.-Y., Bird T., Deng G., Mulder D.W., Smyth C., Laing N.G., Soriano E., Pericak-Vance M.A., Haines J., Rouleau G.A., Gusella J.S., Horvitz H.R. and Brown R.H.Jr. (1993). Mutations in Cu/Zn superoxide dismutase gene are associated with familial amyotrophic lateral sclerosis. Nature 362, 59-62.

Sen C.K. and Packer L. (1996). Antioxidant and redox regulation of gene transcription. FASEB J. 10, 709-720.

Siddique T., Figlewicz D.A., Pericak-Vance M.A., Haines J.L., Rouleau G., Jeffers A.J., Sapp P., Hung W.Y., Bebout J., McKenna-Yasek D., Deng G., Horvitz H,R., Gusella J.F., Brown R.H.Jr and Roses A.D. (1991). Linkage of a gene causing familial amyotrophic lateral sclerosis to chromosome 21 and evidence of genetic-locus heterogeneity. N. Engl. J. Med. 324, 1381-1384.

Sunde P.A. and Hoekstra W.G. (1980). Structure, synthesis and function of glutathione peroxidase. Nutr. Rev. 38, 265-273.

Wen S.-T. and Van etten R.A. (1997). The PAG gene product, a stress-induced protein with antioxidant properties, is an Abl SH3-binding protein and a physiological inhibitor of c-Abl tyrosine kinase activity. Gene Dev. 11, 2456-2467.

Westman N.G. and Marklund S.L. (1981). Copper- and zinc-containing superoxide dismutase and manganese-containing superoxide dismutase in human tissues and human malignant tumors. Cancer Res. 41, 2962-2966.

Wong P.C., Pardo C.A., Borchelt D.R., Lee M.K., Copeland N.G., Jenkins N.A., Sisodia S.S., Cleveland D.W. and Price D.L. (1995). An adverse property of a familial ALS-linked SOD1 mutation causes motor neuron disease characterized by vacuolar degeneration of mitochondria. Neuron 14,1105-1116.

Wood Z.A., Poole L.B. and Karplus P.A. (2003). Peroxiredoxin evolution and the regulation of hydrogen peroxide signaling. Science 300, 650-653.

Yeldandi A.V., Kaufman D.G. and Reddy J.K. (1996). Cell injury and cellular adaptations. In: Anderson's Pathology. 10th ed. Damjanov I. and Linder J. (eds). Mosby. St. Louis. pp 357-386.

Accepted February 3, 2006

Yonago Acta medica 2006;49:83–92

Mallory Bodies in Hepatocytes of Alcoholic Liver Disease and Primary Biliary Cirrhosis Contain N^{ε}-(Carboxymethyl)lysine-Modified Cytokeratin, but not those in Hepatic Carcinoma Cells

Masako Kato, Shinsuke Kato*, Seikoh Horiuchi†, Ryoji Nagai†, Yasushi Horie and Kazuhiko Hayashi‡

*Pathology Division, Tottori University Hospital, Yonago 683-8504, *Department of Neuropathology, Institute of Neurological Sciences, Tottori University Faculty of Medicine, Yonago 683-8504, † Department of Medical Biochemistry, Graduate School of Medical and Pharmaceutical Sciences, Kumamoto University, Department of Biochemistry, Kumamoto University School of Medicine, Kumamoto 860-0811 and ‡Division of Molecular Pathology, Department of Microbiology and Pathology, School of Medicine, Tottori University Faculty of Medicine, Yonago 683-8503 Japan*

Mallory bodies (MBs) are intracytoplasmic bodies seen in hepatocytes of alcoholic liver disease, primary biliary cirrhosis and hepatocellular carcinoma. However, the mechanism of MB formation has not been fully understood. Proteins could be modified to advanced glycation end products (AGEs) after long-term incubation with reducing sugar. AGEs are known to accumulate in several tissues in aging and age-enhanced disorders. To study the possible glycation process in the formation of MBs, hepatocytes of 80 human liver tissues with MBs were subjected to immunohistochemical analyses with five AGEs, two markers for oxidative stress proteins (OSPs) and four stress-response proteins (SRPs). MBs in hepatocytes of primary biliary cirrhosis and alcoholic liver disease were strongly positive for N^{ε}-(carboxymethyl)lysine (CML) and weakly positive for pyrraline. MBs in hepatocellular carcinomas were negative for both CML and pyrraline. No significant immunoreactivity was detected in MBs for other AGEs, such as N^{ε}-(carboxyethyl)lysine, pentosidine, and 3DG-imidazolone, or for OSPs and SRPs. Stainings for cytokeratin, a major protein component of MBs, and CML were co-localized. Furthermore, immunoblot analysis suggested that cytokeratin of MBs was modified to AGE, since a single protein band detected by a monoclonal anti-CML had a molecular weight identical to cytokeratin. The absence of the CML signal in MBs of hepatocellular carcinoma cells could be explained by scarce content of cytokeratin in carcinoma MBs.

Key words: advanced glycation end product; cytokeratin; immunohistochemistry; Mallory body; N^{ε}-(carboxymethyl)lysine

Abbreviations: ABC, avidin-biotin-immunoperoxidase complex; AEC, 3-amino-9-ethylcarbazole; AGE, advanced glycation end product; BSA, bovine serum albumin; CEL, N^{ε}-(carboxyethyl)lysine; CML, N^{ε}-(carboxymethyl)lysine; DAB, 3,3'-diaminobenzidine tetrahydrochloride; HCC, hepatocellular carcinoma; H&E staining, hematoxylin and eosin staining-; HNE, 4-hydroxy-2-nonenal; MB, Mallory body; PAS, periodic acid Schiff; PBC, primary biliary cirrhosis; SDS, sodium dodecyl sulfate; SRP, stress-response protein

Mallory first described cytoplasmic hyaline degeneration in hepatocytes of alcoholic liver cirrhosis (Mallory, 1911). This cytoplasmic hyaline inclusion has been called Mallory body (MB). MB had been thought as specific to alcoholic liver disease (Edmondson, 1986). However, they are also associated with a number of non-alcoholic hepatobiliary diseases, such as Indian childhood cirrhosis, primary biliary cirrhosis (PBC), Wilson's disease, hepatocellular carcinoma (HCC) and adenomatous hyperplasia (Jensen and Gluud, 1994a; Terada et al., 1989). Although several different theories have been proposed for the formation of MBs (Jensen and Gluud, 1994b), the mechanism of MB formation as well as their developmental and pathological significance has remained unknown.

Ultrastructurally MBs consist of aggregates of filaments (Yokoo et al., 1972), and aberrant intermediate filaments of cytokeratin polypeptides (Katsuma et al., 1987). Recently, hyperphosphorylation of cytokeratin 8 and 18 (Stumptner et al., 2000) or ubiquitination of cytokeratin proteins was revealed in MB formation (Yuan et al., 1996). MBs were also known to be positive for αB-crystallin immunohistochemically (Lowe et al., 1992). Namely, MBs contain protein components such as cytokeratin, ubiquitin or αB-crystallin. Furthermore, the other chemical analyses demonstrated that MBs possess carbohydrates (Lyon and Christoffersen, 1971) and reducing sugar (Luisada-Opper et al., 1977) in addition to cytokeratin as the major protein component.

Long-term incubation of proteins with glucose leads, through the formation of early products such as Schiff base and Amadori rearrangement products, to the formation of advanced glycation end products (AGEs). Since monoclonal or polyclonal antibodies against these AGEs have been newly produced, immunological studies using anti-AGE antibodies have demonstrated accumulation of AGE-modified proteins in several human tissues in association with aging (Araki et al., 1992; Kimura et al., 1996) and several disorders such as diabetic complications (Makino et al., 1995), atherosclerosis (Kume et al., 1995) and Alzheimer's disease (Smith et al., 1994). AGE-modification is known to occur in many proteins, especially long-lived proteins, which makes them insoluble, thus enhancing the deposition of modified proteins inside the cells or in the extracellular space (Makino et al., 1995; Giardinò et al., 1996). Finally, AGE-modified proteins that are accumulated in the tissues exhibit direct toxic effects on cells biologically (Vlassara et al., 1994).

AGE-structures reported so far include fluorescent and cross-linking structures such as pentosidine (Sell and Monnier, 1990) and crossline (Nakamura et al., 1992), and nonfluorescent and non-cross-linked structures such as imidazolone (Niwa et al., 1997), N^{ε}-(carboxymethyl)lysine (CML) (Ahmed et al., 1986) and pyrraline (Hayase et al., 1989). The purpose of the present study was to investigate whether AGE-modification could play a role in MB formation. To do this end, human liver tissues with MBs were examined immunohistochemically using antibodies against CML, N^{ε}-(carboxyethyl)lysine (CEL), pyrraline, pentosidine and 3DG-imidazolone. Our results revealed that chemical modification of cytokeratin by CML, a major antigenic AGE-structure, is involved in MB formation in hepatocytes in alcoholic liver disease and primary biliary cirrhosis in contrast to no involvement of CML in MBs in HCC.

Materials and Methods

Patients

Eight hundred liver tissues from autopsy, biopsy and surgical files kept in our Department and Division were surveyed from 1973 to 2000, and MBs were found histologically in 80 cases (8 autopsy cases, 11 biopsy cases and 61 surgical cases). The 80 cases with MBs included three PBC cases (females, aged 37 to 68 years), 17 cases of alcoholic liver disease (15 males and 2 females, aged 33 to 66 years) and 60 cases of HCC (52 males and 8 females, aged 29 to 80 years). Surgical and autopsy specimens of normal liver tissues and other

Table 1. Sources of primary antibodies and dilutions

Antibody	Clonality	Clone	Dilution	Source (reference)
Anti-MB-component protein antibody				
Cytokeratin, broad	Monoclonal		Ready-to-use	Nichirei (Tokyo, Japan)
αB-crystallin	Polyclonal		1:250	J. E. Goldman (Iwaki et al., 1989)
Ubiquitin	Polyclonal		1:1000	S. H. Yen (Lee et al., 1989)
Anti-AGE antibody				
CML	Monoclonal	6D12	0.5 μg/mL	S. Horiuchi (Ikeda et al., 1996)
	Monoclonal	CMS10	0.5 μg/mL	Kumamoto Immunochem. Lab. (Kumamoto, Japan)
Pyrraline	Polyclonal		1.0 μg/mL	S. Horiuchi (Hayase et al., 1989)
Pentosidine	Polyclonal		1.0 μg/mL	S. Horiuchi (Miyata et al., 1996)
CEL	Monoclonal	KNH-30	0.6 μg/mL	Kumamoto Immunochem. Lab. (Kumamoto, Japan)
3DG-imidazolone	Monoclonal	JNH-27	0.5 μg/mL	Kumamoto Immunochem. Lab. (Kumamoto, Japan)
Anti-OSP antibody				
Acrolein	Monoclonal		0.5 μg/mL	NOF (Tokyo, Japan)
4-HNE	Monoclonal		0.5 μg/mL	JICA (Fukuroi, Japan)
Anti-SRP antibody				
SRP27	Monoclonal		Ready-to-use	BioGenex (San Rmon, CA)
SRP32	Monoclonal		1:200	Santa Cruz (Santa Cruz, CA)
SRP72	Monoclonal		1:500	Amersham (Buckinghamshire, United Kingdom)
SRP90	Monoclonal		1:5000	Affinity BioReagent (Neshanic Station, NJ)

AGE, advance glycation end product; CEL, N^{ε}-(carboxyethyl)lysine; CML, N^{ε}-(carboxymethyl)lysine; 4-HNE, 4-hydroxy-2-nonenal; MB, Mallory body; OSP, oxidative stress protein; SRP, stress response protein.

organ tissues from 10 individuals (7 males and 3 females; aged 19 to 68 years) were also examined as controls. The protocols were approved by the Ethics Committee in Tottori University Faculty of Medicine (No. 761).

Histology and immunohistochemistry

After fixation in 10% buffered formalin, the specimens were embedded in paraffin, cut into 4-μm-thick sections and examined by light microscopy. Liver sections were stained by the following routine methods: hematoxylin and eosin (H&E), periodic acid-Schiff (PAS), digestive PAS, silver and azan stainings. The distribution patterns of MBs were classified according to the method of Nakanuma and Ohta (1986). HCCs were graded into grades I, II and III according to the histological grading system of Edmondson and Steiner (1954). Serial sections were used for immunohistochemical analysis. The sources of primary antibodies and their dilutions used are listed in Table 1. Sections were deparaffinized and endogenous peroxidase activity was quenched for 30 min with 0.3% H_2O_2. Sections were then washed in phosphate-buffered saline (PBS), pH 7.4. Normal sera isologous with each secondary antibody were used as blocking reagents. Sections were incubated with one of the primary antibodies or PBS for 18 h at 4°C. As positive controls for CML-immunostaining, atherosclerotic lesions in the wall of aortae from control individuals were used, biopsy specimens of diabetic kidney for pyrraline or pentosidine staining and atherosclerotic tissues also served as positive controls for acrolein and HNE stainings. Some sections were incubated with anti-CML antibody that had been preabsorbed with 1 mg/mL of CML-modified bovine serum albumin (BSA). With respect to the preabsorption test, some sections were incubated with anti-CML, anti-pyrraline, or anti-pentosidine antibody that had been preabsorbed with excess CML-, pyrraline- or pentosidine-modified BSA, respectively. Bound antibodies were visualized by the avidin-biotin-immunoperoxidase complex (ABC) method using the appropriate Vectastain

ABC kit (Vector Laboratories, Burlingame, CA) and 3,3'-diaminobenzidine tetrahydrochloride (DAB) (Dako, Glostrup, Denmark) as the final chromogen. For labeling multiple antigens in the same tissue section, normal and abnormal structures in H&E-stained sections were identified, mapped and photomicrographed. The H&E sections were then decolorized in 70% ethanol containing 1% HCl, after which the sections were rehydrated, quenched for 30 min with 0.3% H_2O_2, rinsed in PBS and incubated with the first primary antibody for 18 h at 4°C. Bound antibody was visualized by the ABC method using 3-amino-9-ethylcarbazole (AEC; Vector Laboratories) as the chromogen, yielding a red product. After photographing the immunoreactive structures, AEC sections were decolorized using 100% ethanol, rinsed twice in PBS and incubated for 60 min at room temperature with glycine-HCl buffer (pH 2.2) to elute the immunoreactive products. The completeness of the elution process was verified by obtaining a negative reaction after reapplication of the appropriate ABC kit including a secondary antibody and AEC on the eluted sections. The sections were subsequently incubated with the second primary antibody for 18 h at 4° C, and immunoreactivity was visualized by the ABC method using DAB as the chromogen. The proportion of positively-immunostained MBs was classified into five different categories; category – means negative staining, category +/– a few MBs were stained weakly, category + less than 10%, category ++ 10–50% and category +++ more than 50%.

Immunoblot analysis

This analysis was carried out on one fresh liver sample of a patient with PBC (Patient 2, a 61-year-old female) and on a liver tissue of age-matched normal individual (a 68-year-old female). In brief, specimens were homogenized in Laemmli sample buffer (Bio-Rad, Hercules, CA) containing 2% sodium dodecyl sulfate (SDS), 25% glycerol, 10% 2-mercaptoethanol, 0.01% bromophenol blue and 62.5 mM Tris-HCl, pH 6.8. The sample was heated at 100°C for 5 min. Soluble protein extracts from the samples were separated on a SDS-polyacrylamide gel (10%–20% gradient, Bio-Rad) and transferred by electroblotting onto Immobilon PVDF (Millipore, Bedford, MA). After blocking with 5% skimmed milk for 30 min at room temperature, the blots were incubated with anti-CML antibody (6D12) overnight at 4°C and visualized with the Vectastain ABC kit and DAB. Appropriate molecular weight markers (Bio-Rad) were included in each run.

Results

Histology and immunohistochemistry

Three cases clinically diagnosed as PBC showed histopathologically liver cirrhosis, biliary (Table 2). The histopathological findings of 17 cases clini-

Table 2. Clinicopathological findings of 20 cases of PBC and ALD with MBs

Case number	Age	Sex	Clinical diagnosis	Histopathology
1	37	F	PBC	LC/biliary
2	61	F	PBC	LC/biliary
3	68	F	PBC	LC/biliary
4	56	M	ALD	Fatty liver
5	44	M	ALD	AH
6	54	M	ALD	AH
7	47	M	ALD	AH
8	61	M	ALD	AH
9	37	M	ALD	Fibrosis
10	47	M	ALD	Fibrosis
11	49	F	ALD	Fibrosis
12	57	M	ALD	Fibrosis
13	65	M	ALD	Fibrosis
14	66	M	ALD	Fibrosis
15	37	F	ALD	LC/septal
16	56	M	ALD	LC/septal
17	59	M	ALD	LC/septal
18	70	M	ALD	LC/septal
19	33	M	ALD	LC/septal
20	61	M	ALD	LC/septal

AH, alcoholic hepatitis; ALD, alcoholic liver disease; F, female; LC/biliary, liver cirrhosis of biliary type (by Havana classification) (Sherlock, 1956); LC/septal, liver cirrhosis of septal type; M, male; MB, Mallory body; PBC, primary biliary cirrhosis.

cally diagnosed as alcoholic liver disease, showed fatty liver (1 case), alcoholic hepatitis (4 cases), liver fibrosis (6 cases) and liver cirrhosis (septal type, 6 cases) by routine stainings (Table 2). Sixty cases of HCCs were classified as the grade I (15 cases), the grade II (41 cases) and the grade III (4 cases). MBs were found predominantly in peripheral areas of regenerative nodules of liver cirrhosis in PBC (Fig. 1A) and alcoholic liver disease, and also in periportal areas of fibrotic alcoholic liver disease. MBs were scattered in fatty liver and in alcoholic hepatitis. MBs in HCCs were found in the cancer tissues (Fig. 1B). The ratio of MB-bearing hepatocytes to total hepatocytes varied from a few to ~10 percent in liver fibrosis, liver cirrhosis and HCCs. The distribution patterns of MBs of PBC were classified as diffuse type (2 cases) and sparse type (1 case). The patterns of MBs of alcoholic liver disease were classified as diffuse type (2 cases) and as sparse type (15 cases). The patterns of MBs of HCCs were as clustering type (21 cases), diffuse type (26 cases) and sparse type (13 cases) (Table 3).

The shape of MBs in PBC and alcoholic liver disease showed granular (Fig. 2A), staghorn, or circlar pattern (Fig. 2D). In contrast, the shape of MBs in HCCs was irregular (Fig. 1B). MBs of alcoholic liver disease, PBC and HCCs were

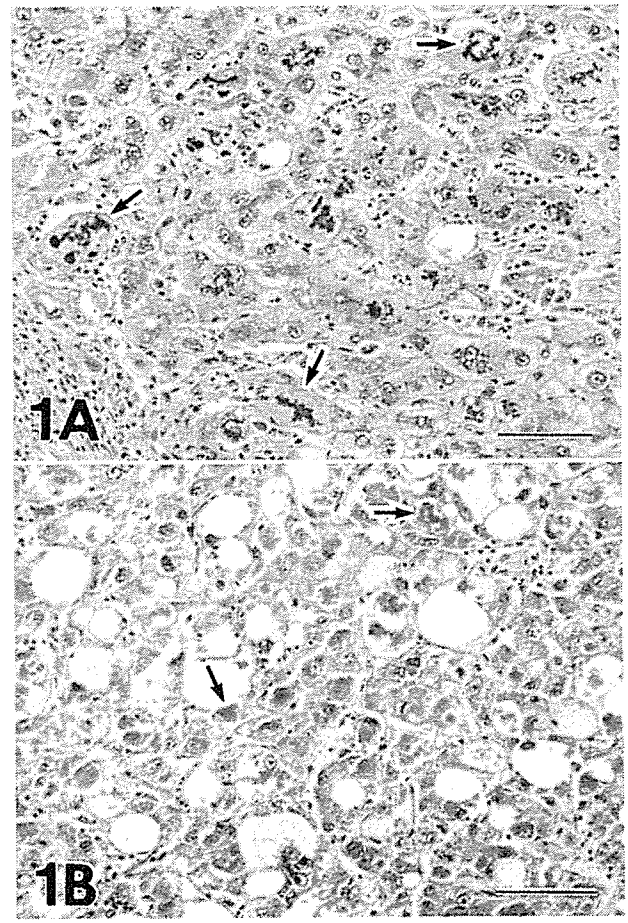

Fig. 1. Hematoxylin and eosin staining of liver tissue of Patient 2 with primary biliary cirrhosis (PBC) (**A**) and the patient with hepatocellular carcinoma (**B**), showing Mallory bodies (MBs) (arrows). Bar = 100 μm.

Table 3. Histopathological and immunohistochemical findings of 80 cases of PBC, ALD and HCC with MBs

	Distribution pattern	Number of cases	CML (6D12)	CML (CMS10)	Pyrraline	Pentosidine	CEL	Cytokeratin
PBC	Clustering	0						
	Diffuse	2	+~+++	+~+++	+/–~–	–	–	++
	Sparse	1	+	+	–	–	–	++
Alcoholic liver disease	Clustering	0						
	Diffuse	2	+~++	+~++	+/–	–	–	++
	Sparse	15	+	+	+/–~–	–	–	++
Hepatocellular carcinoma	Clustering	21						
	Diffuse	26	–	–	–	–	–	+/–
	Sparse	13	–	–	–	–	–	+/–

CEL, N^{ε}-(carboxyethyl)lysine; CML, N^{ε}-(carboxymethyl)lysine; MB, Mallory body; PBC, primary biliary cirrhosis.
Distribution pattern of MBs were divided according to Nakanuma and Ohta (1986).
Proportion of MBs stained positively: +++, > 50%; ++, 10–50%; +, < 10%; +/–, only minor portion.

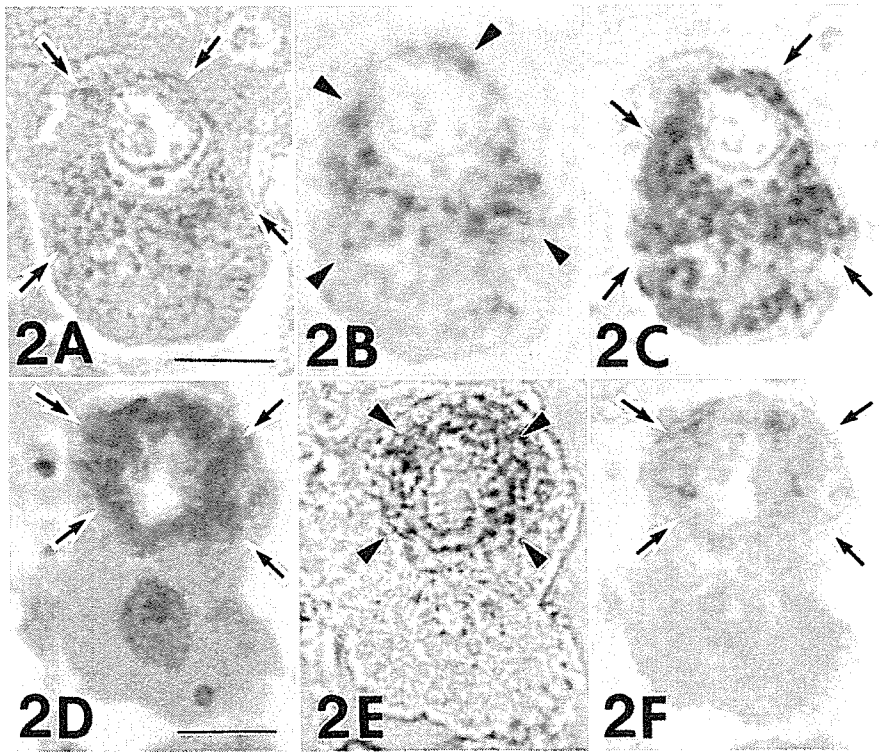

Fig. 2. Light microscopic characteristics of the Mallory bodies (MBs) of Patient 2 with primary biliary cirrhosis.

- **A:** An MB in hematoxylin and eosin (H&E) staining (arrows). Bar = 10 μm (**A–F**: same magnification).
- **B:** The same section as A immunostained for N^{ε}-(carboxymethyl)lysine (CML) using 3-amino-9-ethylcarbazole (AEC) as chromogen (arrowheads).
- **C:** The section used in B was decolorized and restained for cytokeratin using 3,3'-diaminobenzidine tetrahydrochloride (DAB) as chromogen (arrows).
- **D:** An MB in H&E staining (arrows).
- **E:** The section used in D was decolorized and immunostained for CML using AEC as chromogen. A doughnut-shaped MB is stained in red (arrowheads).
- **F:** The section used in E was decolorized and restained for cytokeratin using DAB as chromogen showing the MB (arrows).

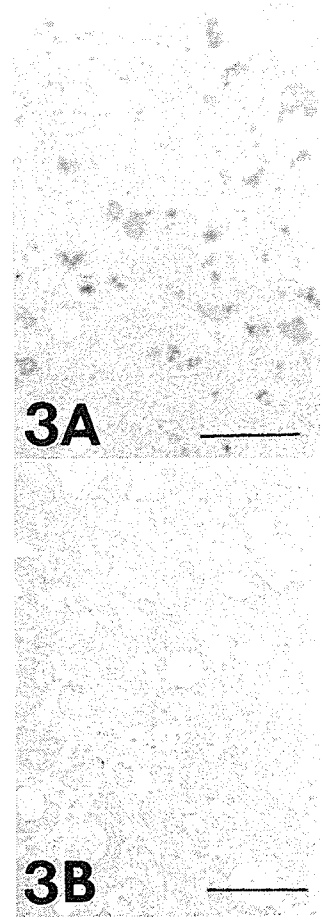

Fig. 3. Liver sections of the patient with hepatocellular carcinoma. Immunostaining for ubiquitin (**A**) and CML (with monoclonal antibody 6D12) (**B**). Bar = 100 μm (**A** and **B**: same magnification).

weakly positive for PAS histochemically (data not shown). The PAS-positivity was confirmed by the digestive PAS staining. MBs in PBC and alcoholic liver disease were confirmed immunohistochemically by positive staining to ubiquitin and αB-crystallin addition to H&E staining. The reaction products within MBs in PBC by the anti-CML antibody exhibited a granular pattern (Fig. 2B) or a circular pattern (Fig. 2E). MBs and MB-bearing hepatic cytoplasm were also stained with the anti-cytokeratin antibody (Figs. 2C and F). The positive reaction products for both CML and cytokeratin were co-localized on the same MBs (Figs. 2B and C; and Figs. 2E and F, respectively).

MBs derived from three cases of PBC and 17 cases of alcoholic liver disease were positively stained to CML (both clone of 6D12 and CMS-10) (Table 3). MBs in one case of PBC and nine cases of alcoholic liver disease were weakly stained with anti-pyrraline antibody. MBs of all cases of both PBC and alcoholic liver disease showed positive for cytokeratin. MBs were not stained by anti-pentosidine antibody, anti-CEL antibody or anti-3DG-imidazolone antibody.

MBs were not stained with antibodies against oxidative stress proteins (OSPs) such as acrolein and HNE nor against stress response proteins (SRPs) (27 kDa, 32 kDa, 72 kDa or 90 kDa) (data not shown). MBs in HCCs were also identified by positive staining to anti-ubiquitin antibody (Fig. 3A). MBs in all cases of HCCs were weakly stained by anti-cytokeratin antibody. By contrast, MBs in HCCs were not stained to CML (Fig. 3B), pyrraline, pentosidine, CEL, 3DG-imidazolone, two types of OSPs (acrolein and HNE) nor four types of SRPs (srp27, 32, 72 and 90). There were no significant differences in AGE-expressions among the histologically different specimens in HCCs.

The proportion of positively-immunostained MBs varied from one sample to another, ranging from less than 10% to more than 50% of total MBs (Table 3). Immunohistochemical stainings of CML of PBC and alcoholic liver disease showed that 1 out of 20 cases was of category +++; 4 out of 20 cases were of category ++, and 15 cases out of 20 cases were of category +. Immunohistochemical stainings of pyrraline of PBC and alcoholic liver disease showed that one case of PBC was of category +/– and nine of 17 cases of alcoholic liver disease were of category +/–. MBs with diffuse distribution pattern were positive for CML or pyrraline more than MBs with sparse type. All cases of PBC and alcoholic liver disease were of category ++ about cytokeratin. All cases of HCC were of category +/– about cytokeratin.

Hepatocytes from 10 control individuals were not stained by five anti-AGE antibodies against either of CML, pyrraline, pentosidine, CEL or 3DG-imidazolone. Similarly, normal hepatocytes showed no immunoreactivities to OSPs, SRPs, αB-crystallin nor ubiquitin. No staining was detected when sections were incubated with PBS. The specificity and high affinity of these antibodies were confirmed by control tissues. As expected (Makino et al., 1995; Kume et al., 1995; Horie et al., 1997), CML-immunoreactivities were observed in smooth muscle cells of atherosclerotic lesions, and immunoreactivities for pyrraline, pentosidine, CEL and 3DG-imidazolone were also noted in the thickening intimae of arteries. As reported earlier (Uchida et al., 1995), macrophage-derived foam cells in the atheromatous lesions were positive for HNE. Anti-CML antibody pretreated with an excess amount of CML-modified BSA did not stain smooth muscle cells in the atherosclerotic lesions. Similarly, anti-pyrraline, or anti-pentosidine antibody pretreated with an excess amount of pyrraline- or pentosidine-modified BSA did not stain the thickening intimae of arteries.

Fig. 4. Western blot analysis using monoclonal CML (with monoclonal antibody 6D12) in liver tissues.

Lane 1: normal control liver.
Lane 2: primary biliary cirrhosis liver (Patient 2).

Immunoblot analysis

The results of immunoblot analyses are shown in Fig. 4. When the liver-tissue homogenate of PBC (Patient 2, a 61-year-old female), whose hepatocytes were demonstrated to contain CML-positive MBs immunochemically, was subjected to immunoblotting with anti-CML antibody, a single band with a molecular weight indistinguishable from that of cytokeratin was detected (Fig. 4). Immunoblotting of the fresh autopsy liver specimen of a normal individual (a 68-year-old female) did not show any specific band (Fig. 4).

Discussion

Although the frequency and the distribution of MBs that were detected by H&E staining were various among 80 cases examined, all of the MBs were positive for ubiquitin, αB-crystallin and cytokeratin immunohistochemically. MBs in HCCs were weakly positive for cytokeratin, but MBs in PBC and alcoholic liver disease were strongly positive for cytokeratin. The present immunohistochemical results coincide with the previous reports which demonstrated that MBs consisted of aggregates of cytokeratin filaments (Yokoo et al., 1972) or that cytokeratin protein of MBs was ubiquitinated (Yuan et al., 1996). In the present study, the facts that MBs contain cytokeratin, ubiquitin and αB-crystallin as protein components were confirmed immunohistochemically.

The novel finding of the present study is that MBs in PBC and alcoholic liver disease were positive for CML and pyrraline in contrast to those of HCCs. In cases of PBC and alcoholic liver disease, immunohistochemical results of the same paraffin sections using anti-CML and anti-cytokeratin antibodies, revealed that both CML and cytokeratin were co-localized on the same MBs. These results suggest that MBs in PBC and alcoholic liver disease have epitopes of CML addition to cytokeratin. No CML-positive reactivities except MBs were found in the liver sections of PBC, alcoholic liver disease, HCCs and normal controls. Furthermore, immunoblot analysis with anti-CML antibody supported the immunohistochemical findings. Single band with a molecular weight about 55 kDa was detected in the liver-tissue homogenate of PBC. This result demonstrated that liver tissue-homogenate of PBC contain CML-combined protein with molecular weight about 55 kDa. Considering the fact that the molecular weight of ubiquitin, one of protein components of MBs is about 8 kDa (Lee et al., 1989; Lowe and Mayer, 1990) and that of αB-crystallin is also 22 kDa (Iwaki et al., 1989), it was suggested that CML-combined protein might be cytokeratin.

Glycation is one of biochemical reactions and it occurs when proteins were incubated with reducing sugars. Finally, CML, CEL or pyrraline-combined proteins through several steps by glycation form AGEs. Although oxidation is necessary for the formation of AGEs in vitro (Nagai et al., 1997), the intention level of oxidation, the nature of oxidative processes, and the period of oxidative stresses are of different in vivo. At the cellular level, living cells can induce a diverse group of SRPs in response to different types of biological stresses, including oxidative damage (Morimoto et al., 1990). Since OSPs and SRPs in MBs were not detected in the present immunohistochemical studies, the amounts of these compounds in MBs might be, if any, negligible, suggesting that the oxidative stress that generates these marker compounds does not contribute to the process of MB formation in vivo.

Modification by glycation occurs in many proteins in relation to the pathogenesis of diseases such as atherosclerosis (Kume et al., 1995), diabetic complications (Makino et al., 1995), Alzheimers' disease (Smith et al., 1994). Furthermore, AGEs are common to be long-lived, insoluble molecules, readily deposited in cells that have a direct cytotoxic effect (Vlassara et al., 1994). Although several hypotheses of MBs have been discussed (Jensen and Gluud, 1994a, 1994b) the results of the present study clarified that AGE-modification of cytokeratin, a major protein component of MBs, plays an important role in the formation of MBs in hepatocytes in the PBC and the alcoholic liver disease. Taken together with abnormal cytokeratin aggregation toxicity, it is conceivable that the AGE modification of cytokeratin in MBs could amplify the aggregation of cytokeratin and that the formation of the AGEs could result in greater toxicity in hepatocytes-bearing MBs in patients with the PBC and alcoholic liver disease. Considering the facts that MBs of HCCs contain less amount of cytokeratin protein, HCC cells form MBs for a short disease duration of tu-

morigenesis or have abnormal biological metabolism, AGE-modification do not contribute to the formation of the MBs in HCC cells. To elucidate the differences between AGE-expressions of alcoholic liver disease or PBC and AGE-expressions of HCCs, a further complete understanding of the molecular mechanisms of MB formation in hepatocytes will be necessary. Our results suggest that the formation of AGEs might be cytotoxic to MB-containing hepatocytes in PBC and alcoholic liver disease in contrast to HCCs.

Acknowledgments: The authors express their appreciation to Dr. James E. Goldman (Department of Pathology, Columbia University), for providing the antibody to αB-crystallin and to Dr. S.-H. Yen (Department of Neuroscience, Mayo Clinic), for donating the antibody to ubiquitin.

This study was supported in part by a Grant-in-Aid for Scientific Research (c) from the Ministry of Education, Culture, Sports, Science and Technology of Japan (SK: 17500229), a Grant From Research on Psychiatric and Neurological Disease and Mental Health (SK) and a Research Grant on Measures for Intractable Diseases from the Ministry of Health, Labour and Welfare of Japan (SK).

References

1 Ahmed MU, Thorpe SR, Baynes JW. Identification of N^{ϵ}-carboxymethyllysine as a degradation product of fructoselysine in glycated protein. J Biol Chem 1986;261:4889–4894.

2 Araki N, Ueno N, Chakrabarti B, Morino Y, Horiuchi S. Immunochemical evidence for the presence of advanced glycation end products in human lens proteins and its positive correlation with aging. J Biol Chem 1992;267:10211–10214.

3 Edmondson HA. Alcoholic liver disease. In: Peters RL, Craig JR, eds. Liver pathology. New York: Churchill Livingstone; 1986. p. 255–283.

4 Edmondson HA, Steiner PE. Primary carcinoma of the liver. A study of 100 cases among 48900 necropsies. Cancer 1954;7:462–503.

5 Giardino I, Edelstein D, Brownlee M. BCL-2 expression or antioxidants prevent hyperglycemia-induced formation of intracellular advanced glycation endproducts in bovine endothelial cells. J Clin Invest 1996;97:1422–1428.

6 Hayase F, Nagaraj RH, Miyata S, Njoroge FG, Monnier VM. Aging of proteins: immunological detection of a glucose-derived pyrrole formed during Maillard reaction in vivo. J Biol Chem 1989;263:3758–3764.

7 Horie K, Miyata T, Maeda K, Miyata S, Sugiyama S, Sakai H, et al. Immunohistochemical colocalization of glycoxidation products and lipid peroxidation products in diabetic renal glomerular lesions. Implication for glycoxidative stress in the pathogenesis of diabetic nephropathy. J Clin Invest 1997;100:2995–3004.

8 Ikeda K, Higashi T, Sano H, Jinnouchi Y, Yoshida M, Araki N, et al. N^{ϵ}-(Carboxymethyl)lysine protein adduct is a major immunological epitope in proteins modified with advanced glycation end products of the Maillard reaction. Biochemistry 1996;35:8075–8083.

9 Iwaki T, Kume-Iwaki A, Liem RKH, Goldman JE. alphaB-crystallin is expressed in non-lenticular tissues and accumulates in Alexander's disease brain. Cell 1989;57:71–78.

10 Jensen K, Gluud C. The Mallory body: morphological, clinical and experimental studies (part 1 of a literature survey). Hepatology 1994a;20:1061–1077.

11 Jensen K, Gluud C. The Mallory body: theories on developmental and pathological significance (part 2 of a literature survey). Hepatology 1994b;20:1330–1342.

12 Katsuma Y, Swierenga SHH, Khettry U, Marceau N, French SW. Changes in the cytokeratin intermediate filament cytoskeleton associated with Mallory body formation in mouse and human liver. Hepatology 1987;7:1215–1223.

13 Kimura T, Takamatsu J, Ikeda K, Kondo A, Miyakawa T, Horiuchi S. Accumulation of advanced glycation end products of the Maillard reaction with age in human hippocampal neurons. Neurosci Lett 1996;208:53–56.

14 Kume S, Takeya M, Mori T, Araki N, Suzuki H, Horiuchi S, et al. Immunohistochemical and ultrastructural detection of advanced glycation end products in atherosclerotic lesions of human aorta with a novel specific monoclonal antibody. Am J Pathol 1995;147:654–667.

15 Lee S, Park YD, Yen SH, Ksiezak-Reding H, Goldman JE, Dickson DW. A study of infantile motor neuron disease with neurofilament and ubiquitin immunocytochemistry. Neuropediatrics 1989;20:107–111.

16 Lowe J, Errington DR, Lennox G, Pike I, Spendlove I, Landon M, Mayer RJ. Balooned neurons in several neurodegenerative diseases and contain alphaB crystallin. Neuropathol Appl Neurobiol 1992;18:341–350.

17 Lowe J, Mayer RJ. Ubiquitin, cell stress and diseases of the nervous system. Neuropathol Appl Neurobiol 1990;16:281–291.

18 Luisada-Opper AV, Kanagasundaram N, Leevy CM. Chemical nature of alcoholic hyalin. Gastroenterology 1977;73:1374–1376.

19 Lyon H, Christoffersen P. Histochemical study of

Mallory bodies. Acta Path Microbiol Scand 1971;79 (Section A):649–657.
20 Mallory FB. Cirrhosis of the liver. Five different types of lesions from which it may arise. Bull Johns Hopkins Hosp 1911;22:69–75.
21 Makino H, Shikata K, Hironaka K, Kushiro M, Yamasaki Y, Sugimoto H, et al. Ultrastructure of non-enzymatically glycated mesangial matrix in diabetic nephropathy. Kidney Int 1995;48:517–526.
22 Miyata T, Taneda S, Kawai R, Ueda Y, Horiuchi S, Hara M, et al. Identification of pentosidine as a native structure for advanced glycation end products in β_2-microglubulin-containing amyloid fibrils in patients with dialysis-related amyloidosis. Proc Natl Acad Sci USA 1996;93:2353–2358.
23 Morimoto RI, Tissie'res A, Georgopoulos C. The stress response, function of the proteins, and perspectives. In: Morimoto RI, Tissie'res A, Georgopoulos C, eds. Stress Proteins in Biology and Medicine. Cold Spring Harbor: Cold Spring Harbor Laboratory Press; 1990. p. 1–36.
24 Nagai R, Ikeda K, Higashi T, Sano H, Jinnouchi Y, Araki N, et al. Hydroxyl radical mediates N^{ε}-(carboxymethyl)lysine formation from Amadori product. Biochem Biophys Res Commun 1997;234:167–172.
25 Nakamura K, Hasegawa T, Fukunaga Y, Ienaga K. Cross-lines A and B as candidates for the fluorophores in age- and diabetes-related cross-linked proteins, and their diacetates produced by Maillard reaction of α-*N*-acetyl-L-lysine with D-glucose. J Chem Soc Chem Commun 1992;14:992–994.
26 Nakanuma Y, Ohta G. Expression of Mallory bodies in hepatocellular carcinoma in man and its significance. Cancer 1986;57:81–86.
27 Niwa T, Katsuzaki T, Ishizaki Y, Hayase F, Miyazaki T, Uematsu T, et al. Imidazolone, a novel advanced glycation end product, is present at high levels in kidneys of rats with streptozotocin-induced diabetes. FEBS Lett 1997;407:297–302.
28 Sell DR, Monnier VM. End-stage renal disease and diabetes catalyze the formation of a pentose-derived crosslink from aging human collagen. J Clin Invest 1990;85:380–384.
29 Sherlock S. Report of the board for classification and nomenclature of cirrhosis of the liver. 5th Pan-American Congress of Gastroenterology. La Havana, Cuba. Gastroenterology 1956;31:213–216.
30 Smith MA, Taneda S, Richey PL, Miyata S, Yan S-D, Stern D, et al. Advanced Maillard reaction end products are associated with Alzheimer disease pathology. Proc Natl Acad Sci USA 1994;91:5710–5714.
31 Stumptner C, Omary MB, Fickert P, Denk H, Zatloukal K. Hepatocyte cytokeratins are hyperphosphorylated at multiple sites in human alcoholic hepatitis and in a mallory body mouse model. Am J Pathol 2000;156:77–90.
32 Terada T, Hoso M, Nakanuma Y. Mallory body clustering in adenomatous hyperplasia in human cirrhotic livers: report of four cases. Hum Pathol 1989;20:886–890.
33 Uchida K, Itakura K, Kawakishi S, Hiai H, Toyokuni S, Stadtman ER. Characterization of epitopes recognized by 4-hydroxy-2-nonenal specific antibodies. Arch Biochem Biophys 1995;324:241–248.
34 Vlassara H, Bucala R, Striker L. Biology of disease. Pathogenic effects of advanced glycosylation: biochemical, biologic, and clinical implications for diabetes and aging. Lab Invest 1994;70:138–151.
35 Yokoo H, Minick OT, Batti F, Geoffrey K. Morphologic variants of alcoholic hyalin. Am J Pathol 1972;69:25–40.
36 Yuan QX, Marceau N, French BA, Fu P, French SW. Mallory body induction in drug-primed mouse liver. Hepatology 1996;24:603–612.

Received September 4, 2006; accepted 10 November, 2006

Corresponding author: Masako Kato, MD

Acta Neuropathol (2006) 112: 52–63
DOI 10.1007/s00401-006-0056-x

ORIGINAL PAPER

Hisae Sumi · Seiichi Nagano · Harutoshi Fujimura
Shinsuke Kato · Saburo Sakoda

Inverse correlation between the formation of mitochondria-derived vacuoles and Lewy-body-like hyaline inclusions in G93A superoxide-dismutase-transgenic mice

Received: 31 May 2005 / Revised: 12 February 2006 / Accepted: 12 February 2006 / Published online: 27 April 2006

Abstract In G93A mice, the most popular model of amyotrophic lateral sclerosis (ALS), neuronal Lewy-body-like hyaline inclusions (LBHIs) and mitochondria-derived vacuoles are observed in addition to motor neuron loss. Although LBHIs are thought to be toxic, the significance of the mitochondria-derived vacuoles has not been fully investigated. In this study, the relationship between the formation of these vacuoles and LBHIs was clarified statistically in the lumbar segment from two phyletic lines of G93A mice (G1L, G1H), using immunohistochemical methods. Furthermore, the distributions of vacuoles and LBHIs were examined in the pons including the facial nucleus, where pathological changes occur in ALS patients and G93A mice. Numerous vacuoles 2–3 μm in diameter were detected in the neuropil of the lumbar segment from G1L mice euthanatized approximately 3.5 months prior to the onset of the disease. Most of the vacuoles disappeared, but some became larger as the disease progressed. The number of vacuoles with a diameter exceeding 5 μm began to decrease after disease onset, while that of intra-neuritic LBHIs increased rapidly. There was a strong inverse correlation between the numbers of vacuoles and LBHIs in symptomatic mice ($P < 0.01$; G1L, $r = -0.91$; G1H, $r = -0.93$). In the facial nucleus of G1L mice, where the number of motor neurons was significantly reduced, only a few LBHIs were detected along with prominent vacuole formation. In contrast, significantly more LBHIs with little vacuole formation were evident around the facial nucleus in G1L mice. Furthermore, the SOD1 immunoreactivity in vacuoles initially increased and then decreased after disease onset. Taken together, the present findings suggest that the mitochondria-derived vacuoles might prevent the formation of LBHIs by sequestering mutated SOD1 from the cytoplasm.

Keywords Vacuole · Lewy-body-like hyaline inclusion · Mitochondria · Transgenic mice · Amyotrophic lateral sclerosis

H. Sumi (✉) · S. Nagano · H. Fujimura · S. Sakoda
Department of Neurology D-4, Osaka University Graduate School of Medicine, 2-2, Yamadaoka, Suita, 565-0871 Osaka, Japan
E-mail: hasumi@neurol.med.osaka-u.ac.jp
Tel.: +81-6-68793571
Fax: +81-6-68793579

S. Kato
Department of Neuropathology, Institute of Neurological Sciences, Faculty of Medicine,
Tottori University, Yonago, Japan

Introduction

Amyotrophic lateral sclerosis (ALS) is a fatal motor neuron disease whose pathogenesis remains unknown. About 10% of ALS cases are familial and approximately 15–20% of familial ALS patients possess the copper/zinc superoxide dismutase (SOD1) gene mutation [8, 40]. Since transgenic mice or rats carrying the human mutated SOD1 gene (SOD1 mice or rats) develop progressive motor deficits caused by loss of anterior horn cells [3, 12, 16, 32, 39, 56], they have been used by many researchers as a model of ALS. SOD1 mice or rats carrying different mutated SOD1 genes have been reported to show different pathologic features: in G93A mice or rats, many Lewy-body-like hyaline inclusions (LBHIs) and mitochondria-derived vacuoles are observed [6, 7, 32]; in G85R or G86R mice, many LBHIs, but almost no vacuoles, appear long before the onset of the disease [3, 39]; in H46R rats, many LBHIs and very few vacuoles are found [32]; in G37R mice, there is prominent vacuole formation and almost no LBHIs [55, 56]. Although in G85R mice the level of mutant G85R SOD1 protein expressed is only 20% of endogenous SOD1, these mice show very progressive motor deficits [3]. Other SOD1

mice or rats express a mutant protein level approximately 10 times higher than that in murine SOD1 [12, 16, 32, 56]. Several lines of G93A or G37R mice with different levels of mutant protein expression show different pathologic features [6, 7, 56]. Thus, the differences in neuropathology observed among SOD1 mice or rats appear to depend on the character of the mutant protein and its level of expression.

SOD1-positive LBHIs in neurons are neuropathological hallmarks of familial ALS linked with SOD1 mutation [15, 17, 22, 44]. In cell lines transfected with mutated SOD1, aggregations of mutated SOD1 or LBHI-like structures are formed [9, 21, 46]. In SOD1 mice or rats, such aggregates of SOD1 or LBHIs appear before onset of the disease [3, 4]. These aggregates of SOD1 or LBHIs, which are found specifically in the affected spinal cord or brainstem [15, 44, 54], are resistant to strong detergents or reducing agents. Although formation of aggresomes [21] or inclusions such as Lewy bodies in Parkinson's disease might be considered the result of cell-protective responses to various forms of stress [36], aggregation of mutant SOD1 or the formation of LBHIs in SOD1-mutated ALS is reported to have a toxic effect [4, 5, 23] due to sequestration of the components that are essential for maintaining cell functions [24, 25], induction of repetitive misfolding and reduction of chaperone function [2], or reduction of the activity of the proteasome integral for protein turnover [20, 21, 53].

The most important function of mitochondria in cells is the production of ATP, which is indispensable for sustaining life. Cytochrome *c* oxidase (CCO), which is located in the inner membrane of the mitochondrion and, in mammals, is composed of 13 different subunits, participates in electron transport within mitochondria [50]. Cytochrome *c* (cyt *c*) is oxidised by CCO through electron transport in the intermembrane space of the mitochondrion [38]. The large amount of energy required for action potentials in neurons depends on the ATP produced by mitochondria through electron transport. In G93A mice, the most widely used animal model of ALS, one of the very early pathologic features is the appearance of vacuoles followed by that of abnormal mitochondria [6, 14, 28, 42, 43], suggesting that the vacuoles are derived from mitochondria [14, 28].

The formation of LBHIs has been thought to have toxic effects, but the significance of the vacuoles remains unclear. Since the vacuoles appear far earlier than the LBHIs, an investigation of vacuoles would be important for clarifying the pathogenesis of the disease in G93A mice. In the study presented here, we carried out a quantitative examination of the vacuoles using an immunohistochemical method and analyzed the relationship between the vacuoles and the formation of LBHIs in the lumbar segment or facial nucleus of G93A mice in order to clarify the significance of mitochondria-derived vacuoles.

Materials and methods

Animals

Transgenic mice expressing the G93A mutated human SOD1 gene at a low (B6SJL-TgN[SOD1-G93A]1Gur^{dl}, G1L) or high (B6SJL-TgN[SOD1-G93A]1Gur, G1H) level were obtained from the Jackson Laboratory (Bar Harbor, ME, USA). These mice were bred and maintained as hemizygotes by mating with wild-type B6SJL mice. Non-transgenic littermates were used as controls. All animals were genotyped using polymerase chain reaction amplification of the tail DNAs under conditions that have been described previously [33]. All animals were handled in accordance with the Guidelines for the Care and Use of Laboratory Animals at Osaka University Graduate School of Medicine. We evaluated the animals clinically, examining their hindlimb extension when they were suspended in the air by the tail [1, 33, 34, 49].

Tissue preparation

We examined control (260 ± 6 days old), G1L, and G1H mice ($n = 3$ in each group). G1L mice were euthanatized at the age of 90, 140 (the asymptomatic stage), 180 (the presymtomatic stage), 230 days (the symptomatic stage) or at the end stage when they could hardly move or drink water because of severe paralysis (259 ± 6 days old, the moribund state). G1H mice were euthanatized at the age of 66 (the asymptomatic stage), 100 (the early symptomatic stage), or 115 days (the late symptomatic stage). They were deeply anesthetized with sodium pentobarbital, and perfused with phosphate-buffered saline (PBS, pH 7.4) followed by 4% paraformaldehyde. The brainstem and spinal cord were removed, immersed in the same fixative overnight at 4°C, and then cryoprotected. Ten-micrometer-thick frozen sections were prepared and stained with hematoxylin and eosin (HE). Small pieces of lumbar segments were fixed with 2.5% glutaraldehyde in 0.1 M PB (pH 7.4) for 2 h at 4°C, followed by 1% osmium tetroxide in 0.1 M PB at 4°C, dehydrated in an ethanol series and embedded in Epon; LUVEAK-812 (glycerol triglycidyl ether, Nakarai Tesque, Kyoto, Japan)/LUVEAK-DDSA (dodecylsuccinic anhydride, Nakarai Tesque)/LUVEAK-MNA (methylnadic anhydride, Nakarai Tesque)/LUVEAK-DMP-30 (2,4,6-Tris (dimethylaminomethyl) phenol, Nakarai Tesque). Transverse sections 1 μm thick were stained with toluidine blue.

Immunohistochemical analysis of vacuoles in lumbar segment and brainstem

For immunohistochemical evaluations, frozen or deparaffinized sections were incubated for 30 min with

0.3% H_2O_2 to quench endogenous peroxidase activity and then washed with PBS. Normal goat serum was used as a blocking reagent. Mouse monoclonal antibodies against cyt *c* (1:100 in 1% PBS containing bovine serum albumin, clone 6H2.B4, BD PharMingen, CA, USA), CCO subunit I (1:400 clone 1D6, Molecular Probes Inc, OR, USA), human SOD1 (0.5 μg/ml, clone 1G2, MBL, Aichi, Japan) or GFAP (ready to use, DAKO, Glostrup, Denmark) were used as primary antibodies. Tissue sections were incubated with each primary antibody for 18 h at 4°C. The avidin–biotin–immunoperoxidase complex (ABC) method was employed according to the manufacturer's instructions to detect each bound antibody using the appropriate Vectastain ABC kits (Vector Laboratories, Burlingame, CA, USA). 3,3′-Diaminobenzidine tetrahydrochloride (DAKO, Glostrup, Denmark) was used as the final chromogen. Hematoxylin was used to counterstain cell nuclei. In control experiments, primary antibodies were omitted from the incubation medium.

Quantitative evaluation of motor neurons, LBHIs and cyt *c*-positive vacuoles in the lumbar segment

To estimate the number of neurons in the gray matter (VII, VIII, IX Rexed areas) showing clear nucleoli and cell bodies with a diameter greater than 25 μm [26, 28, 48], presumed to be alpha motoneurons [10, 30, 31], video images of the anterior horns were obtained with a digital camera (KEYENCE VB-7010, KEYENCE, Osaka, Japan) attached to a light microscope (ECLIPSE E800, Nikon, Tokyo, Japan) for each section, and the areas of motor neurons showing clear nucleoli and cell bodies were measured using image analysis software (VH-H1A5, KEYENCE). The number of neurons with a diameter greater than 25 μm were counted in HE-stained sections. LBHIs with a halo and core and cyt-*c*-positive vacuoles in the gray matter were also counted (×100 objective). LBHIs were also confirmed using antibodies against human SOD1 and GFAP. Since the vacuoles are contained exclusively in neuronal processes [19, 43], and not in astrocytes, only neuronal LBHIs were counted to examine the relationship between the vacuoles and LBHIs in neurons. LBHIs in cells possessing glial nuclei were omitted. To establish how the size and number of vacuoles in the lumbar segments of G1L mice changes chronologically over the clinical course of the disease, vacuoles were divided according to size into small (<5 μm) or large (>5 μm). Every fifth section (40 μm interval) was obtained, and three sections from each mouse were used to obtain the total number of neurons, LBHIs or vacuoles. The quantitative evaluation was analyzed statistically. Moreover, the relationship between the number of vacuoles and LBHIs was estimated in each symptomatic mouse (G1L, 230 days and the moribund state 259 ± 6 days; G1H, 100 and 115 days).

Quantitative analysis of LBHIs in the pons including the facial nucleus

For histological analyses of the facial nucleus (nVII), we examined non-transgenic littermates ($n=3$, 264 ± 7 days) and G1L mice in the moribund state ($n=7$, 258 ± 7 days). Each carefully hemisected brainstem was embedded in paraffin and sectioned transversely. The pons including the nVII was identified in these sections, with reference to the mouse brain atlas of Paxinos and Franklin [37]. Six-micrometer-thick paraffin sections were prepared and stained with HE. In the nVII, large neurons with clear nucleoli and cell bodies were counted. LBHIs located in three subregions of the pons (vacuole-rich area = intra-nVII, the border zone, and vacuole-poor area, as delineated in Fig. 1) were also counted (×40 objective). To estimate the number of LBHIs per unit area in each subregion, video images of the pons were obtained with a digital camera (KEYENCE VB-7010, KEYENCE, Osaka, Japan) attached to a light microscope (ECLIPSE E800, Nikon, Tokyo, Japan) for each section, and the areas of three subregions were measured using image analysis software (VH-H1A5, KEYENCE). Every fifth section (at 24-μm intervals)

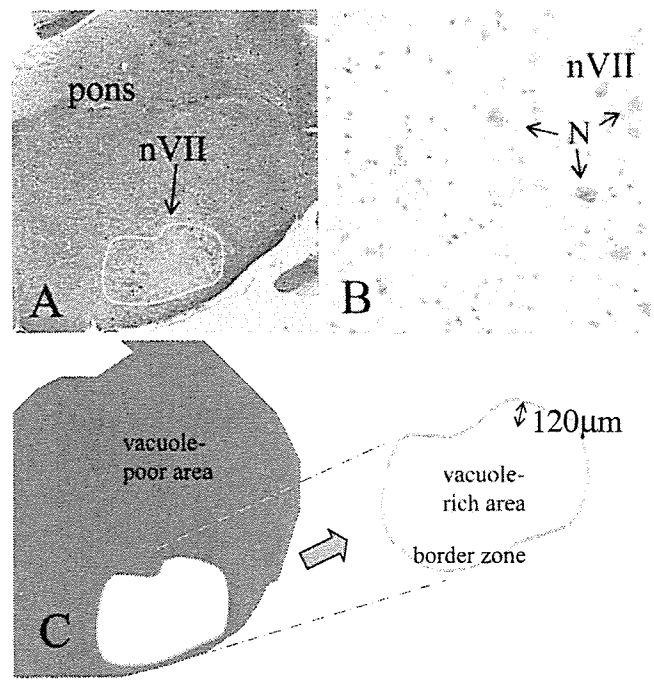

Fig. 1 Schematic diagram of the three subregions in the pons; vacuole-rich area (= intra-nVII), the border zone and vacuole-poor area. The boundary of massive vacuole formation limited to the facial nucleus (nVII) is shown at low (**a**) and high (**b**) magnification as a *yellow line*, using actual microscopic fields digitized for illustrative purposes. The definition of the vacuole-rich area (= intra-nVII), border zone and vacuole-poor area is as follows: vacuole-rich area (*light blue*) corresponds to the inner area outlined in *yellow*; the border zone (*white*) corresponds to the surrounding area outlined in *yellow and green*, 120 μm exterior to the *yellow line*; the vacuole-poor area (*pink*) corresponds to the outer area of the pons excluding the other two regions. *N* neuron

was obtained, and three sections from each mouse were used to obtain the total number of neurons and the density of LBHIs. The number of motor neurons and the density of LBHIs were analyzed statistically. All quantitative investigations were performed independently by three neuropathologists (HS, HF, SK).

Statistics

Data are expressed as the mean ± standard error of the mean (SEM). All statistical analyses of histopathological data were carried out using the Statview for Macintosh software package (Ver5.0, SAS Institute Inc, CA, USA). A nonparametric test, Mann–Whitney *U* test, was used to analyze the number of neurons, LBHIs and vacuoles in the lumbar segment or the number of neurons and the density of LBHIs in the pons. The relationship between the number of LBHIs and vacuoles in the lumbar segment was estimated by regression analysis.

Results

Morphological changes of vacuoles in the lumbar segment of G1L or G1H mice

Many tiny vacuoles 2–3 μm in diameter were found in neurites mainly at the edge of the anterior horn in G1L mice at 90 days (Fig. 2a). Some of the vacuoles were hardly distinguishable from capillary vessels. At 140 days, larger but fewer vacuoles than those at 90 days were observed in the same area (Fig. 2b). Vacuoles were also scattered diffusely in the anterior horn. At 180 days, round vacuoles larger than those at 140 days (Fig. 2c) were frequently found throughout the gray matter. At the later stages in G1L mice, the large vacuoles appeared slightly deformed and were reduced in number (Fig. 2d). Many LBHIs were scattered in the gray matter. In G1H mice, more prominent vacuole formation was observed (Fig. 4a, d) than that in G1L mice. The vacuoles became larger and their number was reduced by 115 days (Fig. 4d) in comparison with those at 100 days (Fig. 4a). Although at 100 days the vacuoles were observed mainly in the anterior horn, by 115 days their distribution had also extended to the whole of the gray matter.

Immunohistochemical analyses of vacuoles in the lumbar segment of G1L mice

As a negative control, sections were incubated without the primary antibody; this resulted in no staining in the lumbar segments of normal and G93A low-copy transgenic mice (G1L mice). As expected, the cytoplasm of motor neurons was clearly stained for cyt *c* or CCO in the lumbar segment of normal mice (Fig. 3a, b). The staining pattern with the two antibodies was similar, showing a fine granular pattern. The neuropil was also weakly stained for these antibodies. The immunohistochemical analysis revealed many tiny vacuoles, strongly positive for cyt *c* at the edge of the anterior horn in G1L mice (90 days; Fig. 3c–e). Some vacuoles were scattered in the neuropil of the anterior horn. Axons were lined with tiny vacuoles that appeared to be attached together. The rim of the vacuoles in the neuropil was stained for cyt *c* (Fig. 3d, e). The structures lying interior to the vacuolar rim were CCO-positive, although the rim itself was CCO-negative. At 140 days, the number of vacuoles was lower than that at 90 days. In contrast, large vacuoles (> 5 μm), which were never seen at 90 days, were frequently observed at the edge of the anterior horn (Fig. 3f). The cyt *c* immunoreactivity was reduced within the rim of these large vacuoles (Fig. 3f, g). Small vacuoles (< 5 μm) did

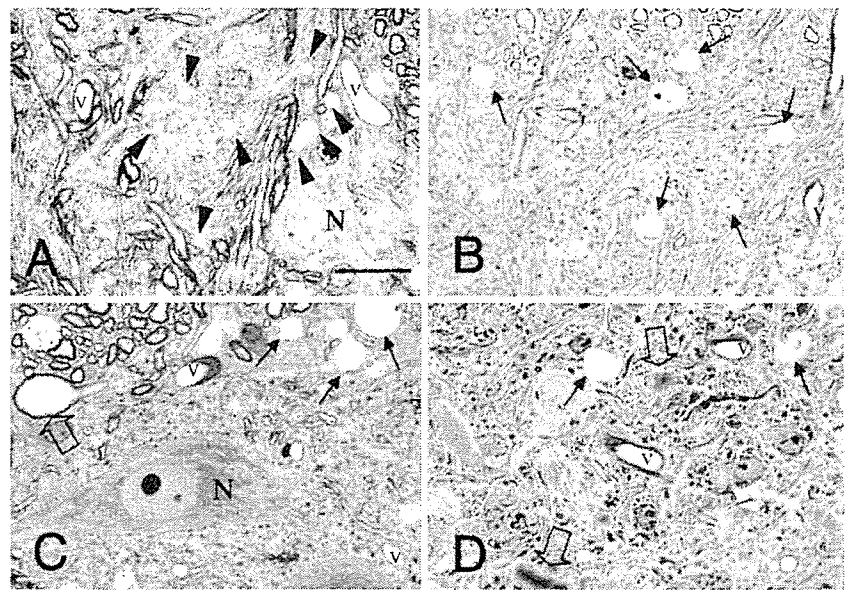

Fig. 2 Morphological changes in vacuoles in the anterior horn of G1L mice at different stages. (Epon sections, toluidine blue, **a** 90 days, **b** 140 days, **c** 180 days, **d** end stage). **a** Many small vacuoles (< 5 μm, *arrow heads*) are evident at the edge of the anterior horn. **b** The number of vacuoles has decreased. Vacuoles (*arrows*) at the edge of the anterior horn have become larger. **c** The number of vacuoles (*arrows*) is smaller than in **b**. Note the large vacuoles in neurites including axons (*clear arrow*). **d** Only a few vacuoles (*arrows*) are evident. LBHIs (*clear arrow*) appear in the anterior horn. *N* neuron; *V* vessels. Scale bar **a** (also for **b**–**d**) 20 μm

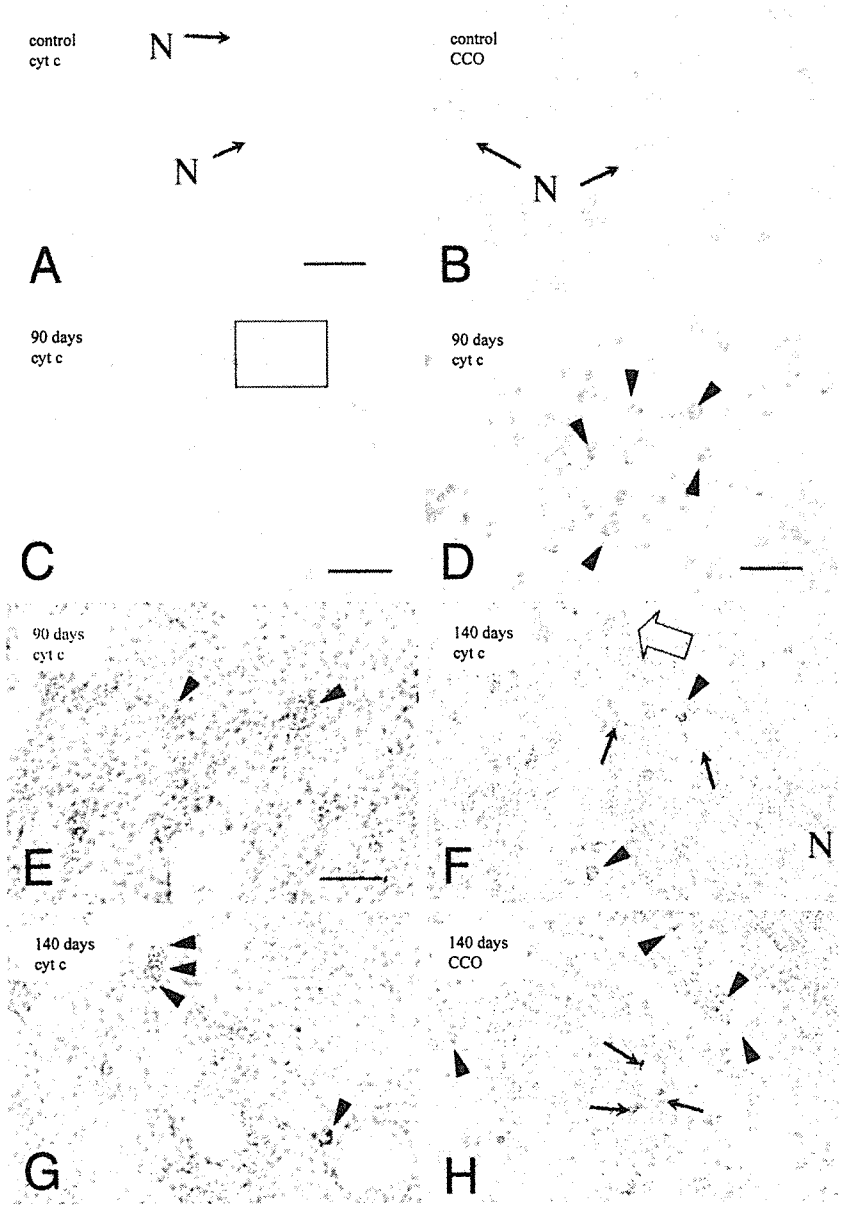

Fig. 3 Immunohistochemistry of vacuoles in the anterior horn of G1L mice (**a**, **b** normal control, **c–l** G1L mice; **a**, **b** 263 days, **c–e** 90 days, **f–h** 140 days, **i** 180 days, **j**, **k** 230 days, **l** end stage; **a**, **c–g**, **j**, **l** cyt *c*, **b**, **h**, **i**, **k** CCO). **a** A fine granular staining pattern is evident in the cytoplasm of motor neurons (*N*, *arrows*). The neuropil is also weakly stained. **b** Motor neurons (*N*, *arrows*) show well-defined cytoplasmic staining for CCO. Diffusely scattered fine dots can be seen in the neuropil. **c–e** Tiny, densely immunolabeled vacuoles within the rim (*arrow heads*) are prominent at the edge of the anterior horn. **d** is a high magnification view of **c**. **e** is a high magnification view of **d**. **f** The number of vacuoles is lower than in **d**. Large vacuoles (> 5 μm, *arrows*), which were never seen in **d**. The immunoreactivity for cyt *c* is reduced within the rim of large vacuoles (*arrows*) compared to that of small vacuoles (< 5 μm, *arrow heads*). In axons, tiny vacuoles are tightly packed to form a columnar shape (*clear arrow*). **g** is a high magnification view of **f**. **h** Abnormal structures lying interior to the rim of vacuoles (*arrows*, *arrow heads*) are strongly positive for CCO. Irregular CCO-positive dots (*arrow heads*) are scattered in the neuropil. **i** Large CCO-positive complexes lying interior to the rim of large vacuoles. **j** The number of vacuoles (*arrow*, *arrow head*) is lower than that in **i**. Cyt-*c*-positive small vacuoles (*arrow head*) are seen only rarely. **k** CCO-positive complexes (*arrows*) lying interior to the vacuolar rim have become atrophic in comparison with those in **i**. **l** Small vacuoles are not evident. Some large vacuoles (*arrows*) remain. *N* neurons; *V* vessels. Scale bars: **a** (also for **b**)50 μm, **c** 100 μm, **d** (also for **f**, **h–l**) 20 μm, and **e** (also for **g**) 10 μm

not fuse to form a large vacuole. Some small and large vacuoles were found in the dorsal horn. Each vacuole had CCO-positive structures lying interior to the rim (Fig. 3h). At 180 days, there was a reduction in the number of small vacuoles (< 5 μm), and many large vacuoles (> 5 μm) were found scattered not only at the edge of the anterior horn, but also throughout the neuropil. These vacuoles had highly CCO-positive structures lying interior to the rim (Fig. 3i). At later stages, the tiny, strongly cyt *c*-positive vacuoles were

Fig. 3 (Contd.)

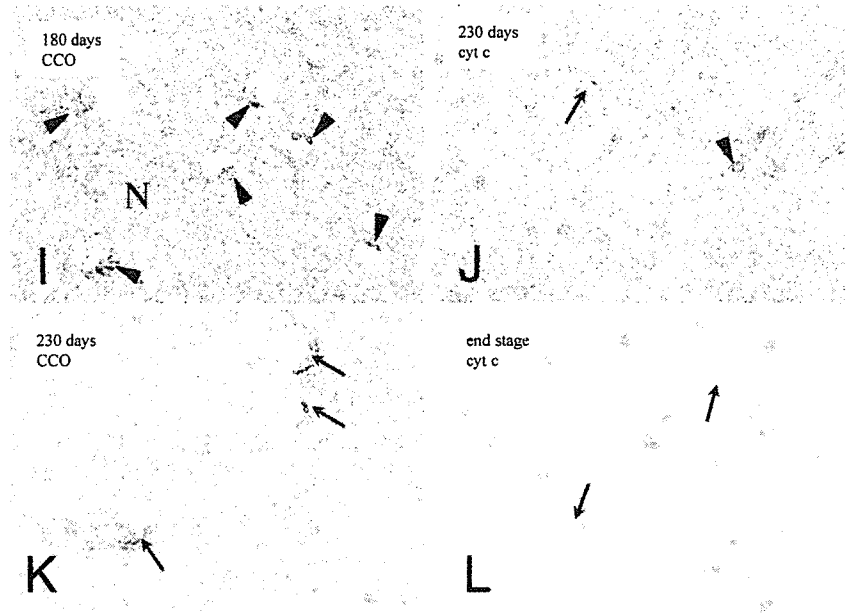

seen only rarely (Fig. 3j, l), and some large vacuoles were observed scattered throughout the neuropil. The CCO-positive structures lying interior to the vacuole rim became atrophic (Fig. 3k), especially in moribund mice. Cyt *c*-positive vacuoles were never seen in the soma of neurons from G1L mice.

Immunohistochemical analyses of vacuoles in the lumbar segment of G1H mice

In symptomatic G1H mice (100 and 115 days), prominent vacuole formation was observed (Fig. 4b, c, e, f). The vacuolar rims were cyt-*c*-positive and there were

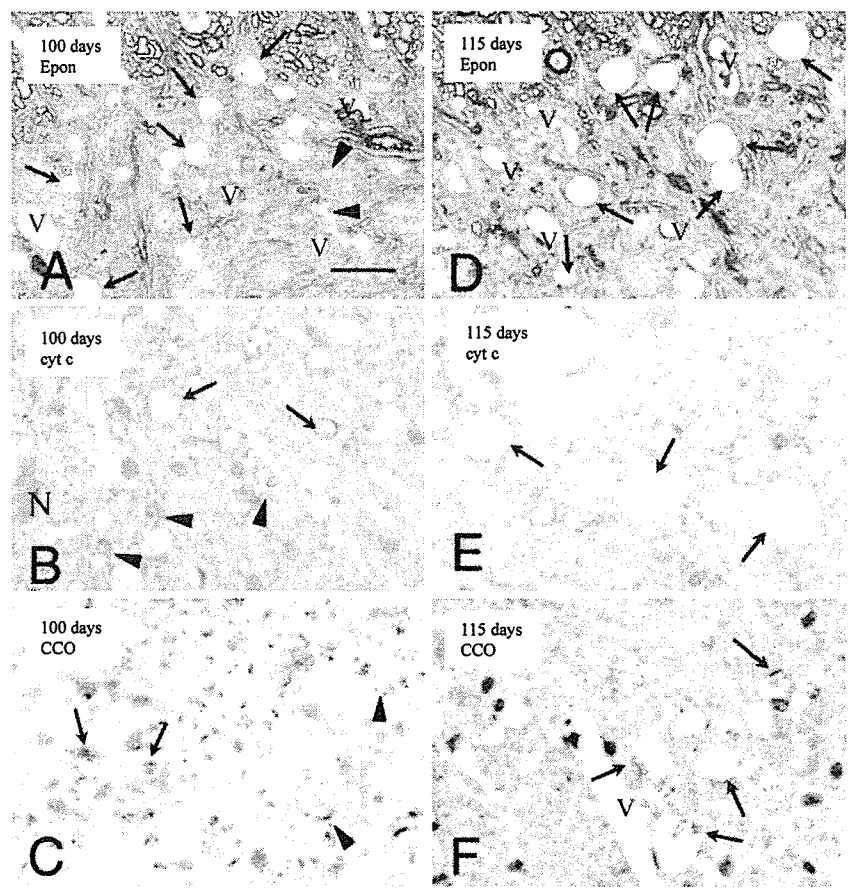

Fig. 4 More prominent vacuole formation with similar immunostaining patterns for cyt *c* and CCO in the anterior horn of G1H mice (**a–c**; 100 days, **b–f**; 115 days, **a**, **d**; Epon sections, toluidine blue, **b**, **e**; cyt *c*, **c**, **f**; CCO). **a** Abundant small (< 5 μm, *arrow heads*) or large (> 5 μm, *arrows*) vacuoles are present in neurites. **b** Cyt-*c*-positive staining in the rim of small (*arrow heads*) and large (*arrows*) vacuoles. The immunoreactivity of the large vacuoles (*arrows*) is reduced, as in G1L mice. **c** CCO-positive structures are evident in small (*arrow heads*) or large vacuoles (*arrows*). **d** The number of vacuoles is reduced. Larger vacuoles than those in **a** are frequently evident. **e** Large vacuoles about 15–20 μm in diameter (*arrows*) are observed more frequently than in the G1L lumbar segment. **f** Somewhat atrophic CCO-positive structures (*arrows*) lying interior to the rim of large vacuoles. *N* neurons; *V* vessels. Scale bar, **a** (also for **b–f**) 20 μm

CCO-positive structures lying interior to them, as observed in G1L mice. Cyt *c* immunoreactivity was reduced in the large vacuoles (Fig. 4b, e). The structures lying interior to the vacuolar rim, evident at 100 days (Fig. 4c), became rather atrophic by 115 days (Fig. 4f). At 100 days, the ratio of the number of large vacuoles (> 5 μm) to the total number of vacuoles was more than 50% (Fig. 4b); this figure had reached almost 90–100% by 115 days (Fig. 4e). The vacuoles in G1H mice tended to be larger than those in G1L mice.

Quantitative analysis of the vacuoles, LBHIs and motor neurons in the lumbar segment of G1L and G1H mice

Figure 5 shows the number of small (< 5 μm) and large (> 5 μm) vacuoles, and LBHIs and motor neurons (> 25 μm) in the lumbar segment during the clinical course of the disease in G1L mice. Numerous small vacuoles were already evident at 90 days, and their number decreased as the disease progressed (Fig. 5a, Table 1, $P < 0.05$). The number of large vacuoles, which appeared at around 140 days, were increased significantly by 180 days but then decreased significantly by 230 days (Fig. 5a, Table 1, $P < 0.05$). The ratio of the number of large vacuoles to the total number of vacuoles was 10–20% at 140 and 180 days, and ~50% in moribund mice (Fig. 5a). In G1H mice, the total number of vacuoles showed a tendency to decrease, but not to a significant degree (Table 1, $P = 0.1266$). The number of neurons declined significantly after 180 days in G1L mice, and after 66 days in G1H mice (Table 1, $P < 0.05$). LBHIs were restricted to the anterior horn at 180 and 100 days in G1L and G1H mice, respectively, becoming more widespread at the later stages. The number of LBHIs increased significantly in G1L or G1H mice as the disease progressed (Fig. 5b, Table 1, $P < 0.05$). Most of the LBHIs were intra-neuritic.

Correlation between the numbers of vacuoles and LBHIs in symptomatic G1L and G1H mice

Figure 6 shows the correlation between the numbers of vacuoles and LBHIs observed in symptomatic G1L (230 days and in the moribund state) and G1H (100 and 115 days) mice. The number of vacuoles in G1H mice was greater than in G1L mice. Regression analysis revealed a statistically significant inverse correlation between the numbers of vacuoles and LBHIs in both G1L ($r = -0.91$, $P < 0.01$) and G1H ($r = -0.93$, $P < 0.01$) mice.

Quantitative analysis of LBHIs in the nVII and the differential localization of LBHIs and vacuoles

HE staining revealed atrophic motor neurons with prominent vacuole formation in the nVII of moribund G1L mice. Most of the vacuoles in the nVII (Fig. 7b)

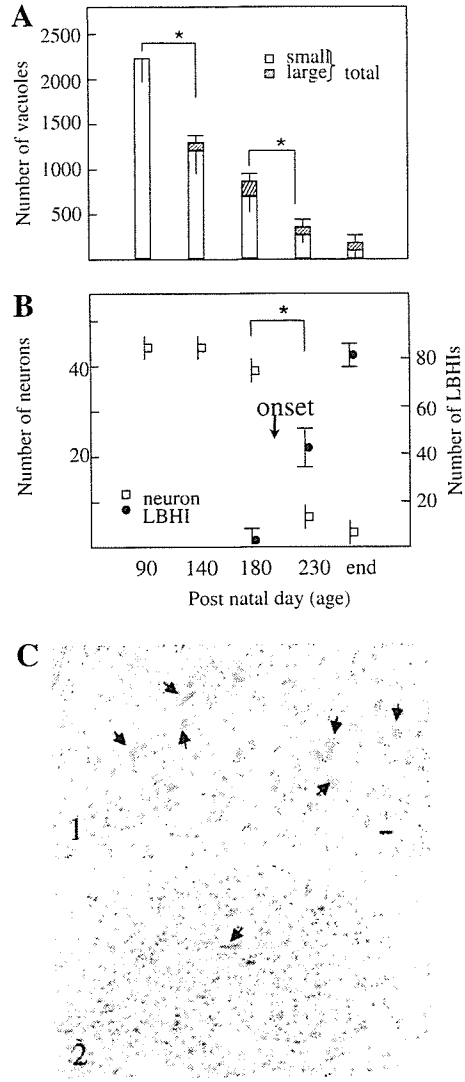

Fig. 5 Time course of changes in the number of vacuoles (**a**), LBHIs and motor neurons (**b**) in the anterior horn of G1L mice. **a** Numerous small vacuoles are evident at 90 days. The number of small vacuoles decreases significantly with disease progression (*$P < 0.05$). The large vacuoles are present from 140 days, and their number then increases significantly by 180 days, followed by a significant decrease by 230 days. **b** The number of neurons (> 25 μm) declines significantly after 180 days (*$P < 0.05$) and, conversely, the number of LBHIs increases significantly after 180 days (*$P < 0.05$). Data are presented as mean ± SEM ($n = 3$ for each group). **c** Representative hematoxylin and eosin (HE) staining of the anterior horn in control (**1**) and G1L mice at the end stage (**2**). The number of neurons (> 25 μm, *arrows*) is reduced in (**2**). Scale bar **c** 25 μm

were larger than those observed in the lumbar segment. The number of motor neurons in the nVII was significantly reduced (Table 2, $P < 0.05$), and LBHIs were found only rarely in the vacuole-rich area (= intra-nVII). In marked contrast, LBHIs were found frequently in the border zone (see Materials and methods), but there were very few vacuoles (Fig. 7c). Most of the vacuoles were located in the neuropil, and not in the soma of neurons (Fig. 7d). Most of the LBHIs were also